crystals

MDPI

Article

Mineral Vesicles and Chemical Gardens from Carbonate-Rich Alkaline Brines of Lake Magadi, Kenya

Melese Getenet [1], Juan Manuel García-Ruiz [1,*], Cristóbal Verdugo-Escamilla [1] and Isabel Guerra-Tschuschke [2]

[1] Laboratorio de Estudios Cristalográficos, Instituto Andaluz de Ciencias de la Tierra (CSIC-UGR), Avenida de las Palmeras 4, Armilla, E-18100 Granada, Spain; dessie.melese@csic.es (M.G.); cristobal.verdugo@csic.es (C.V.-E.)

[2] Centro de Instrumentación Científica, Universidad de Granada (UGR), 18071 Granada, Spain; iguerra@ugr.es

* Correspondence: juanmanuel.garcia@csic.es; Tel.: +34-958-230-000 (ext. 190201)

Received: 28 April 2020; Accepted: 28 May 2020; Published: 1 June 2020

Abstract: Mineral vesicles and chemical gardens are self-organized biomimetic structures that form via abiotic mineral precipitation. These membranous structures are known to catalyze prebiotic reactions but the extreme conditions required for their synthesis has cast doubts on their formation in nature. Apart from model solutions, these structures have been shown to form in serpentinization-driven natural silica-rich water and by fluid-rock interaction of model alkaline solutions with granites. Here, for the first time, we demonstrate that self-assembled hollow mineral vesicles and gardens can be synthesized in natural carbonate-rich soda lake water. We have synthesized these structures by a) pouring saturated metal salt solutions, and b) by immersing metal salt pellets in brines collected from Lake Magadi (Kenya). The resulting structures are analyzed by using SEM coupled with EDX analysis, Raman spectroscopy, and powder X-ray diffraction. Our results suggest that mineral self-assembly could have been a common phenomenon in soda oceans of early Earth and Earth-like planets and moons. The composition of the obtained vesicles and gardens confirms the recent observation that carbonate minerals in soda lakes sequestrate Ca, thus leaving phosphate behind in solution available for biochemical reactions. Our results strengthens the proposal that alkaline brines could be ideal sites for "one-pot" synthesis of prebiotic organic compounds and the origin of life.

Keywords: Lake Magadi; soda lake; mineral self-organization; mineral vesicles; calcite; witherite; rhodochrosite; chemical gardens; early Earth; prebiotic chemistry; origin of life

1. Introduction

Mineral self-organization is an important subject for understanding pattern formation in Earth and Materials Sciences [1]. Among the different self-organized patterns [2], chemical gardens, specifically silica-induced self-organized structures, are thought to be relevant for the earliest stages of the planet, when alkaline silica-rich oceans evolved from methane-rich to CO and CO_2-rich atmosphere and hydrosphere [3]. Under these geochemical conditions of Hadean Earth, it is thought that mineral membranous structures (mineral gardens), and silica/carbonate biomorphs were forming in the alkaline oceans, rich in silica and/or carbonate. Mineral gardens are hollow tubular mineral membranes formed via abiotic precipitation upon the interaction of metal-ion salts with aqueous solutions containing anions such as silicate, carbonate, and phosphates [4,5]. It has been shown that the space-compartmentalized silica membranes are small batteries [6] that selectively catalyze the synthesis of prebiotically relevant compounds such as carboxylic acids, amino acids, and nucleobases in the presence of formamide [7].

So far, mineral gardens have only been synthesized using laboratory model solutions, except for two cases where silica gardens form upon the interaction of model alkaline fluids with granites [8] and the interaction of serpentinization-driven natural alkaline water with metal salt pellets [9].

It has been demonstrated that silica-induced mineral self-assembly could have been a common phenomenon on primitive Earth and Earth-like planets [9], where alkaline environments are thought to be widespread. In addition to serpentinization-driven water [9], soda lakes such as Lake Magadi (Kenya) are proposed as having the naturally high alkalinity and high silica content required to trigger mineral self-organization [3,10]. It has also been suggested that Precambrian oceans were in some way analogous to modern soda lakes such as Lake Magadi [3,11–14]. Recent work [15] has shown that carbonate-rich lakes are highly plausible environments for accumulating phosphate at concentration and pH levels relevant to laboratory syntheses of prebiotic organophosphate compounds. This is due to calcium sequestration in carbonate minerals that prevent apatite precipitation and accumulate phosphate [15]. Therefore, testing the geochemical plausibility of self-organization in one of the early Earth-analogous environments, soda lakes, is important for prebiotic chemistry and life detection. Calcium-based mineral self-organization experiments in carbonate-rich soda lake water have two advantages: testing geochemical plausibility of mineral self-assembly and testing the role of carbonate-rich water in calcium sequestration. Up until now, there have been no reported self-assembled mineral membranes synthesized in natural modern soda lakes.

Therefore, we have tested the precipitation of self-assembled mineral membranes from Lake Magadi brines, in Southern Kenya. Lake Magadi is one of the soda lakes of the East African Rift Valley, with the characteristics of high pH, silica and carbonate concentration [16,17]. It occupies a narrow trough formed by N-S faulting of plateau trachyte during the Pleistocene. The predominant geology of the Lake Magadi area is alkali trachyte lava flows [18,19]. A unique combination of tectonic, volcanic, hydrothermal and climatological settings favor soda lake formation in East Africa [20]. Geochemical studies of closed-basin water in volcanic terrains show that their chemical composition is mainly controlled by silicate hydrolysis and evaporative concentration [21,22]. We have performed two types of membrane precipitation experiments. The first type is mineral garden precipitation by immersing pressed metal (Ba, Ca, Co, Cu, Mg, Mn, Fe (II), Fe (III) and Zn) salt pellets into Lake Magadi water [4,5] (hereafter, Magadi gardens). The second one is mineral vesicle precipitation by adding drops of saturated solutions of the above metal salts onto Lake Magadi water [23] (hereafter, Magadi vesicles). The focus in this article is Ba, Ca and Mn mineral vesicles synthesized by adding drops of saturated salt solutions onto Lake Magadi water. Hence, here we present the macroscopic growth of mineral gardens and Co, Mg, Zn and Fe (II) vesicles to demonstrate the range of mineral self-organization that might form in soda lakes.

2. Materials and Methods

2.1. Geological Setting, Sampling and Hydrochemical Analysis

Lake Magadi is one of the saline and alkaline soda lakes of the East African Rift Valley. It lies in the axial trough of the southern Kenya Rift Valley formed by the N–S faulting of plateau trachyte during the Pleistocene [18,19]. The predominant geology of the Lake Magadi area is alkali trachyte lava flows [18,19] overlain by Holocene bedded trona and trona-bearing muds [16].

Lake Magadi brine is the last stage of the evolution of dilute inflows enriched in Na^+, SiO_2, and HCO_3^- through hydrolysis of weathered volcanic glass and lavas from the rift escarpments. These inflows lose their Ca and Mg content before joining the groundwater system beneath the rift floor due to evaporative precipitation of alkaline Earth carbonate in the rift floor sediments [17,24]. Through a combination of further rock-water interaction, evaporative concentration and solute loss, the initially dilute water produces highly alkaline groundwater characterized by high pH, Na^+, HCO_3^-, Cl^-, CO_3^{2-} and SiO_2 contents [16,17]. This groundwater reservoir discharges warm and hot springs into Lake Magadi lagoons along its shoreline. Upon surface evaporation and mineral precipitation

(mainly trona), these lagoons form the most fractioned Lake Magadi brines saturated in trona. The high concentrations of SiO_2 are attributed to the dissolution of silicate-rich volcanic rocks by feeder springs and subsequent evaporative concentration accompanied by pH rise [25]. Hydrothermal input is an important contributor to silica in soda lake waters [20]. The high pH of Lake Magadi brines attributes to trona deposition and subsequent depletion in HCO_3^- and CO_2 degassing [16,17].

The sample used for the experiments was collected from the Lake Magadi evaporation ponds during the field campaign in March 2018. The sample was collected and stored in polyethylene bottles. The sampling point was located at a coordinate of 199441E and 9791457N (UTM) and 602m above sea level. The in-situ pH was measured to be 10.9. The in-situ temperature was 37 °C. The hydrochemistry of the Lake Magadi sample was analyzed by ALS Laboratory Group SL, except for Na^+, K^+, SO_4^{2-}, and F^-. Cl^-, CO_3^{2-}, and HCO_3^- were analyzed by potentiometric titration. Total P and SiO_2 were determined by discrete spectrophotometry. Ca^{2+}, Ba^{2+}, B^+, Sr^{2+}, and total Fe were analyzed using inductively coupled plasma (ICP) atomic emission spectrometry (AES). Al^{3+}, Mg^{2+}, Br^-, and I^- were determined by using inductively coupled plasma (ICP) mass spectrometry (MS). To avoid matrix interference, samples were homogenized and mineralized with nitric acid in an autoclave under high pressure (7.5 atm) and temperature (170 °C) before analysis by ICP-AES and ICP-MS. Na^+ was analyzed by using inductively coupled plasma (ICP) optical emission spectrometry at the Instrumental Technical Services of the Estación Experimental del Zaidín (CSIC) in Granada (Spain). F^- was measured by the ion-selective electrode technique with a pH and ion-meter GLP 22 CRYSON at the Instituto de Catálisis y Petroleoquímica-CSIC, Madrid (Spain). K^+ and SO_4^{2-} was determined by using Varian Cary 1E ultraviolet-visible spectrophotometry at the Laboratorio de Estudios Cristalográficos (LEC) of the Instituto Andaluz de Ciencias de la Tierra (IACT) in Granada, Spain. Total dissolved solids were determined gravimetrically after filtering the water by using glass microfibre filters (Environmental Express, 1.5 µm pore size). The hydrochemical analysis of Lake Magadi water used for the growth of mineral gardens and vesicles is presented in Table 1.

Table 1. Chemical analysis of the Lake Magadi water used for mineral garden and vesicle synthesis. Elemental concentrations are in ppm, conductivity in mS/cm.

pH	T (°C)	Conductivity	TDS	Na^+	K^+	SiO_2	Cl^-	CO_3^{2-}	HCO_3^-	SO_4^{2-}
10.9	37	16,200	440,000	179,460	831	1080	125,000	54,900	8110	2254
F^-	**PO_4^{3-}**	**Mg^{2+}**	**Al^{3+}**	**Ca^{2+}**	**Fe^{tot}**	**B^+**	**Sr^{2+}**	**Ba^{2+}**	**Br^-**	**I^-**
1075	418	0.023	<0.005	<0.5	<0.05	211	0.0767	0.622	725	26.6

2.2. Magadi Gardens and Vesicles Synthesis

Mineral membranes were synthesized by using two types of experimental procedures. The first procedure is a classical method used in silica garden growth experiments [4]. The method consists of the immersion of crystals of soluble salts into a viscous sodium silicate solution, which form tubular structures (Magadi gardens) through a combination of buoyancy and osmosis. Under this setup, crystalline pellets (13 mm diameter) of $CaCl_2{\cdot}2H_2O$ (Sigma Aldrich ≥ 99%), $BaCl_2{\cdot}2H_2O$ (Sigma Aldrich ≥ 99%), $CoCl_2{\cdot}6H_2O$ (Sigma Aldrich)/$Co(NO_3)_2{\cdot}6H_2O$ (PANREAC), $CuSO_4{\cdot}5H_2O$ (PROBUS ≥ 98%), $CuCl_2{\cdot}6H_2O$ (Sigma Aldrich ≥ 99%), $FeCl_2{\cdot}4H_2O$ (Honeywell Fluka)/$FeSO_4{\cdot}7H_2O$ (Sigma Aldrich), $FeCl_3$ (Honeywell Fluka)/$Fe_2(SO_4)_3{\cdot}9H_2O$ (PROBUS), $MgCl_2{\cdot}6H_2O$ (Sigma Aldrich ≥ 99)/$MgSO_4$ (Sigma Aldrich ≥ 99.5%), $MnCl_2{\cdot}4H_2O$ (Sigma Aldrich), and $ZnSO_4{\cdot}7H_2O$ (PANREAC)/$ZnCl_2$ (Sigma Aldrich ≥ 99) were placed at the bottom of a 10 mL plastic vial by using double-sided tape, and 5 mL of Lake Magadi brine was poured into the vial slowly. The pellets were prepared by grinding the above salts to powder fraction using an agate mortar and then pressing with 3–10 ton pressure.

The second experiment was performed by adding drops of saturated solutions of the metal salts (mentioned above) onto a reservoir of Lake Magadi brine in half-filled Linbro plate wells and plastic

cuvettes [23]. This method of membrane growth gives hollow bulb-like and spherical precipitates (Magadi vesicles) hanging on top of the carbonate-rich water and with an opening towards the water-air interface (atmosphere). Saturated metal salt solutions were prepared by dissolving an excess amount of metal salts into Milli-Q membrane-purified water followed by filtration using a 0.45 µm pore size filter. The pH of these metal salts were measured with CRISON GLP 21 pH meter except for $FeCl_3$ and $ZnCl_2$, which are measured with HANNA HI98160 portable pH meter because of their high acidity. Both of the experimental procedures for the membrane growth were performed under ambient lab conditions.

After the completion of the growth, the membranes are cleaned with distilled water and ethanol multiple times before harvesting from the reservoir. In the case of tubular gardens, the water outside the tube was replaced with distilled water and then ethanol to dry the membrane faster. Mineral vesicles were cleaned by removing the metal salt solution inside the vesicles by introducing a syringe through their "mouth" open to the atmosphere. After the removal of the solution inside the vesicle, the outer solution was removed slowly until the hanging vesicle smoothly lands on the bottom of the wells or the cuvettes. The vesicles were cleaned by repeated addition of distilled water and ethanol outside and inside the vesicle using a syringe. Finally, the mineral vesicles and gardens were collected by using a tiny brush and a spatula.

2.3. Membrane Characterization

The growth process of Magadi gardens and vesicles was monitored by time-lapse photography and video using a Nikon optical microscope and camera respectively. Both top view and lateral view were acquired. After drying at ambient temperature and careful isolation from the reservoir, ex-situ characterization of the texture and chemical composition of the tubular and the vesicular membranes were performed by using a Zeiss Supra 40VP field-emission scanning electron microscope (SEM) equipped with an Oxford energy-dispersive X-ray analyzer (EDX) at the Centro de Instrumentación Científica (CIC) of the University of Granada (Spain) operating at 5–20 keV. Determination of the crystalline phases of the membranes was performed by using a high-resolution Bruker D8 Advance X-ray diffractometer with monochromatic Cu $K_{\alpha 1}$ radiation, primary Ge(111) monochromator and a Lynxeye PSD detector in our lab. Powder diffraction of samples took place in transmission mode, at 40 kV acceleration voltage, and 40 mA current for one hour from 5° to 80° 2θ with an increment of 0.02° per second. Mineral phases were identified by using Bruker AXS Diffrac EVA software with the ICCD PDF-2 and the Crystallographic Open Database. Raman spectra of fragments of the membranes were recorded by using a HORIBA Jobin Yvon LabRAM high-resolution ultraviolet-visible light spectrometer equipped with an Olympus BX41 optical microscope with binocular and Koehler illumination and a charge-coupled device detector at an excitation wavelength of 532 nm (frequency-doubled neodymium-doped yttrium-aluminium-garnet laser).

3. Results

3.1. The Magadi Gardens Growth Process

We have identified three types of Magadi garden growth processes by immersing metal salt pellets in Lake Magadi water. In less soluble and less acidic salts of Ba^{2+}, Mn^{2+} and Fe^{2+} (Table 2), the pellets remain intact inside the growth medium and there was no membrane formation observed due to the inability of the alkaline water to dissolve the metal salts that upon interaction with the anions would form membranes. In the case of Fe^{3+} ($FeCl_3$ and $Fe_2(SO_4)_3{\cdot}9H_2O$), Cu^{2+} ($CuCl_2{\cdot}6H_2O$ and $CuSO_4{\cdot}5H_2O$) and Zn^{2+} ($ZnCl_2$ and $ZnSO_4{\cdot}7H_2O$), the experiment resulted in a premature bursting of the membrane and sedimentation by gravity due to high acidity and high solubility of the metal salts (Table 2). The bursting of the membrane was accompanied by the bubbling of gases (see Videos S1–S3). Unlike the aforementioned metals, the salts of Ca^{2+} ($CaCl_2{\cdot}2H_2O$) and Co^{2+} ($CoCl_2{\cdot}6H_2O$ and $Co(NO_3)_2{\cdot}6H_2O$) form tubular membranes shown in Figures 1 and 2 respectively. Likewise, Mg^{2+}

($MgCl_2{\cdot}6H_2O$) pellets immersed in Magadi water form mineral gardens (not presented here) that are morphologically similar to Co ($Co(NO_3)_2{\cdot}6H_2O$)) gardens.

Table 2. Metal salts used for the mineral vesicles and gardens experiments, their measured pH and solubility in g/100g of water at 25 °C [26]. Accuracy of pH measurements: ±0.1.

Salt	**$BaCl_2{\cdot}2H_2O$**	**$CaCl_2{\cdot}2H_2O$**	**$MnCl_2{\cdot}4H_2O$**	**$CoCl_2{\cdot}6H_2O$**	**$Co(NO_3)_2{\cdot}6H_2O$**
pH	5.2	4.6	2.3	2.6	3.5
Solubility	37	81.3	77.3	56.2	103
Salt	**$CuCl_2{\cdot}6H_2O$**	**$CuSO_4{\cdot}5H_2O$**	**$FeCl_2{\cdot}4H_2O$**	**$FeSO_4{\cdot}7H_2O$**	**$FeCl_3$**
pH	0.5	3.1	1.0	2.6	−1.7
Solubility	75.7	22	65	29.5	91.2
Salt	**$Fe_2(SO_4)_3{\cdot}9H_2O$**	**$MgCl_2{\cdot}6H_2O$**	**$MgSO_4$**	**$ZnCl_2$**	**$ZnSO_4{\cdot}7H_2O$**
pH	−0.3	5.1	8.1	−1.9	4.7
Solubility	440 [1]	56	35.5	408	57.7

[1] Solubility measured at 20 °C.

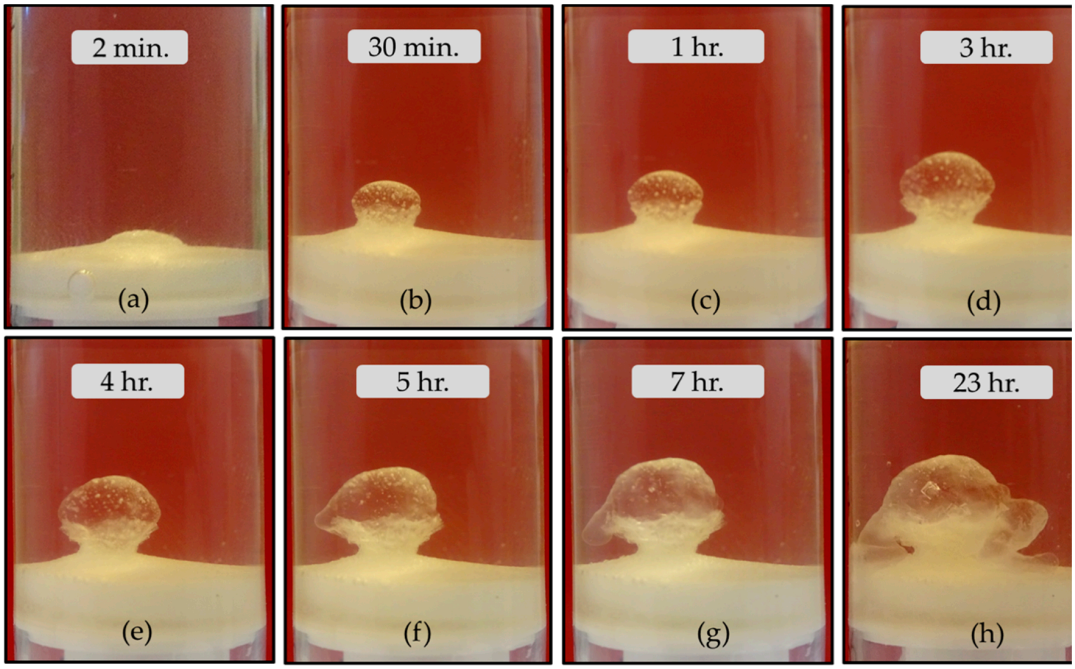

Figure 1. The growth process of calcium carbonate garden. The diameter of the vial is 1.45 cm.

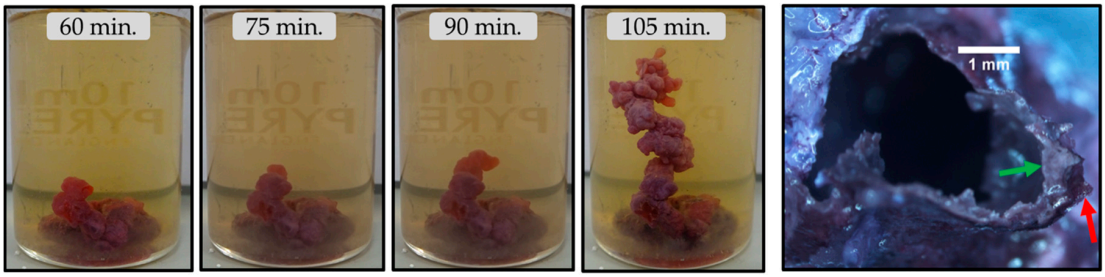

(**a**) (**b**)

Figure 2. Tubular mineral gardens synthesized by immersing cobalt nitrate pellets in Lake Magadi water. (**a**) Time-lapse images of the growth process (diameter of the beaker is 25 mm); (**b**) cross-section of the tubular membrane.

Figure 1, a set of frames taken from Video S4, shows the macroscopic growth of Ca gardens. Upon the interaction of the calcium chloride pellet with Lake Magadi water, a white dome-shaped structure forms (Figure 1a, and Video S4). The osmotic-driven inflow of water into the dome-shaped structure causes gradual swelling and the formation of the transparent elastic membrane at the interface between the outer Magadi water and the inner salt solution. As shown by the morphology of the calcium gardens (Figure 1f–h), the growth process takes place both in vertical and horizontal directions. After the horizontal growth of the membrane, vertically downward growth follows (Figure 1f–h). The combination of these vertical and horizontal membrane growths gives rise to the tubular structure. These tubular structures have a variable diameter (3–7 mm) because of horizontal expansion and their length can reach 6.5 mm. The powder X-ray diffraction shows calcite, gaylussite, pirssonite and trona phases (Figure S1). The powder X-ray diffraction (Figure S1) and a video (Video S4) showing the macroscopic growth are presented in Supplementary Materials.

After the addition of the Magadi water on the Co pellets, a dome-shaped envelope forms surrounding the pellet in about 30 min (Video S5). Due to osmotic-driven diffusion of water, the membranous envelope swells and finally ruptures. The rupture of the envelope ejects the inner Co solution into the surrounding Magadi water, which upon precipitation forms the tubular mineral gardens (Figure 2a). The growth of the tube continues in periodic pulses that range from 6 s to 3 min with an eventual change of growth direction. The change in growth direction produces rounded and tubular branches connected with the main tubular membrane (Figure 2a at 105 min). These small tubular branches give rise to an elliptical cross-section (Figure 2b). The height of cobalt gardens reach ca. 30 mm. Cobalt gardens have two layers (Figure 2b, red and green arrow). The exterior layer is a very thin film (Figure 2b, red arrow). As a result, these membranes are highly fragile and it must be isolated carefully. The powder X-ray diffraction (Figure S2) shows $Co_2(OH)_3Cl$ phase. The powder X-ray diffraction (Figure S2) and a video (Video S5) showing the macroscopic growth are presented in the Supplementary Materials.

3.2. The Magadi Vesicles Growth Process and Characterization

Drops of saturated Fe^{3+}, Cu^{2+} and $ZnCl_2$ solutions undergo premature bursting when they interact with Lake Magadi water (Videos S6–S8). The bubbling of gases was observed during the bursting of the vesicles. When the metal salt drops of Ca^{2+}, Ba^{2+}, Mg^{2+}, Mn^{2+}, Zn^{2+}, Fe^{2+} and Co^{2+} are placed on Lake Magadi water, hollow bulb-like and spherical vesicles form at the interface between the two solutions.

3.2.1. Calcium Chloride Vesicles

Calcium vesicles were synthesized by adding drops of saturated calcium chloride solutions onto Lake Magadi water in a half-filled cuvette. Figure 3a and Video S9 show the growth process of Ca vesicles. Figure 3a is a set of frames taken from Video S9 in Supplementary Materials. The Ca salt drops placed on the surface of Magadi water remain hanging in the uppermost part of the water throughout the growth process (Figure 3a) due to the lower density of the Ca salt solution. The drops change from bulb-like to spherical shape during the first 10 min. During this morphological change, the bottom of each drop lifts up while expanding radially outward. This morphological evolution is accompanied by a color change from transparent to white. Calcium vesicles are hollow mineral membranes formed by mineral precipitation at the interface between the two solutions. These vesicles have an opening ("mouth") at the water–air interface (Figure 3b).

After washing with distilled water and alcohol, vesicles are dried and powdered for X-ray diffraction. The X-ray diffraction shows halite, calcite, trona, vaterite and gaylussite phases (Figure 4). Raman spectra acquired on vesicle fragments after cleaning with a similar protocol confirmed only calcite (Figure S3). The bands at 153 and 280 cm^{-1} are translational and librational modes (lattice modes) of CO_3^{2-} respectively. The bands at 712 and 1085.3 cm^{-1} are assigned to in-plane bending and symmetric stretching (internal modes) of CO_3^{2-} group respectively [27,28]. Trona, vaterite and

gaylussite did not appear in Raman spectra most likely because of low proportion. However, trona, gaylussite and vaterite were observed in SEM micrographs.

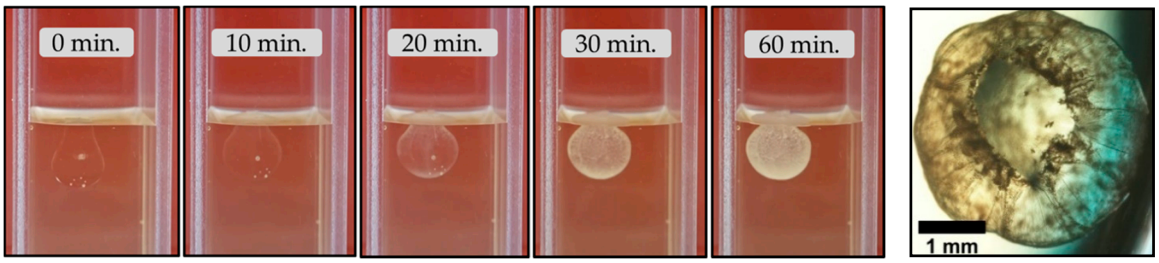

Figure 3. (**a**) Temporal evolution of morphology and texture of the calcium mineral vesicles (width of the cuvette is 1.25 cm); (**b**) hollow calcium vesicle with its opening.

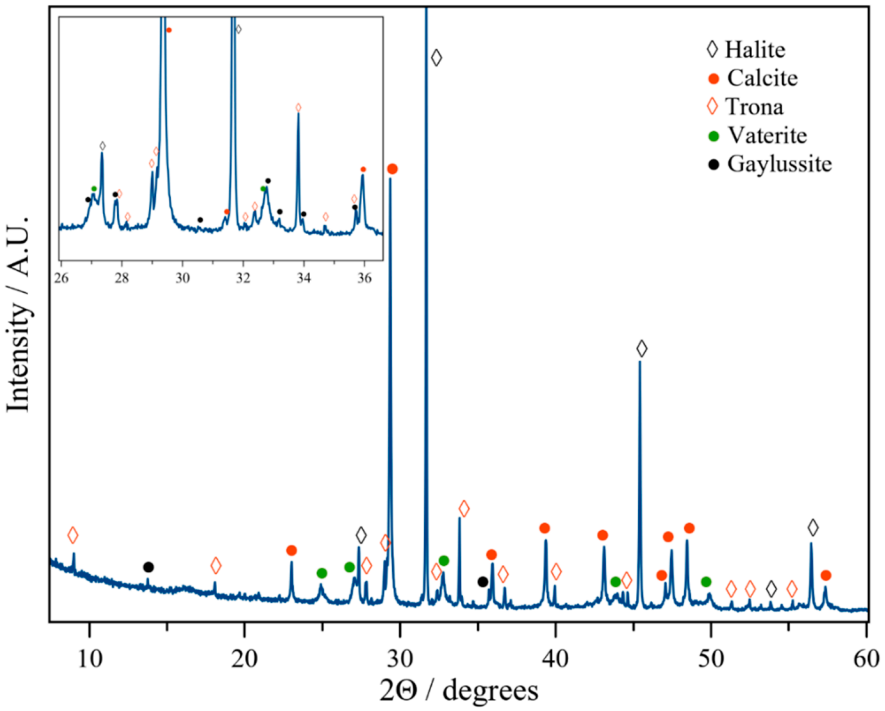

Figure 4. Powder X-ray diffractogram of calcium vesicles.

EDX mapping (Figure 5a and Figure S4) and point analysis (Figure 5b and Figure S5) show that the cross-sections of calcium vesicles are composed of bilayer of calcite with halite core where interlayered calcite precipitate. Figures S4 and S5 in Supplementary Materials show the separate elemental maps of Figure 5a and the EDX analyses of the rectangles in Figure 5b respectively. The calcite bilayers are composed of nano- to few micron-sized spherical aggregates of calcite, which are in turn composed of nano-spherical aggregates. The inner calcite layer is thicker and reach ca. 25 µm thickness (Figure 5a). A thin layer of halite cover the internal wall of calcium vesicles whereas elongated trona crystals precipitate on the external surface of the membranes (Figure 5a). Similar to trona, gaylussite precipitate on the external calcite layer (see Figure 5c and Figure S6 for the point EDX analyses).

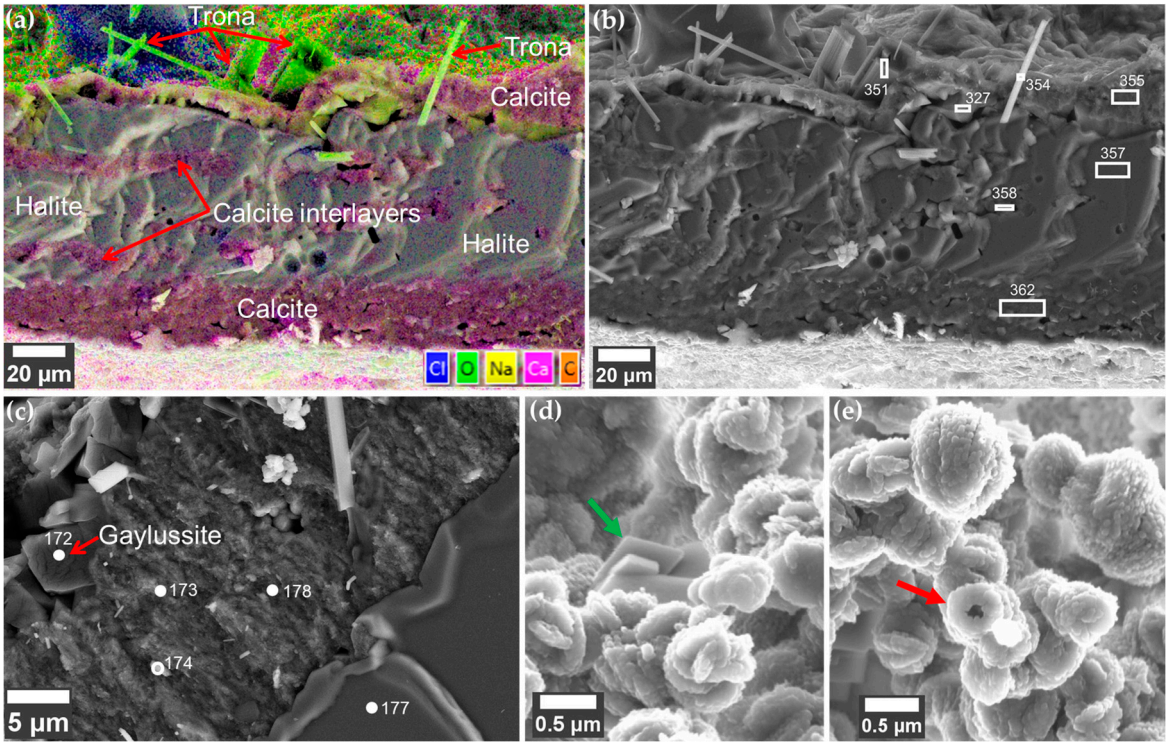

Figure 5. SEM micrographs of calcium vesicles synthesized by adding drops of calcium chloride solution in Magadi water. (**a**) EDX map of the membrane cross-section containing bilayer of calcite, halite core, interlayered calcite and trona on the external surface; (**b**) SEM micrograph of the panel (**a**) with points where EDX analysis was performed (see Figure S5); (**c**) cross-section of the membrane showing gaylussite crystals; (**d**) rhombohedral calcite (green arrow); (**e**) hollow vaterite sphere (red arrow) on the exterior of the membrane.

Aggregates of calcite and vaterite minerals (Figure 5d,e) form small patches on the exterior of the membrane. Due to the fragile nature of calcium vesicles, rupture of the membrane during cleaning may form non-extensive precipitates on the exterior of the membrane when the interior calcium and the exterior carbonate-rich water comes in contact. The dominant minerals in these local patches are spherules of calcite (Figure 5d,e). These local precipitates are also composed of rhombohedral calcite (Figure 5d, green arrow) and vaterite with a hole at the centre (Figure 5e, red arrow).

3.2.2. Barium Chloride Vesicles

Barium vesicles were synthesized by placing drops of saturated barium chloride solution on Magadi water in a half-filled cuvette. Figure 6 and Video S10 show the growth process of Ba vesicles. Figure 6 is a sequence of frames taken from Video S10 (in Supplementary Materials). Upon the interaction of the Ba solution with the Magadi water, barium vesicles immediately precipitate at the interface between the drop and the Magadi water. Consequently, the transparency of the drop changes to white within about a minute. The vesicles remain hanging on the upper part of the water. Later on, these vesicles sink to the bottom of the reservoir (Figure 7a).

After an hour of growth, the lowering and sinking of the opening allow water to enter into the hollow vesicles, which upon interaction with the inner Ba solution form white mineral precipitates inside the vesicles. These white precipitates give rise to sudden and distinct color changes of the vesicles. Following the intrusion of the exterior water, the vesicles sink to the bottom of the cuvettes (Figure 7a). These vesicles develop corrugated surfaces that exist throughout the growth processes (Figures 6 and 7b). Barium vesicles are also hollow mineral membranes with an opening at the air–water interface (Figure 7c).

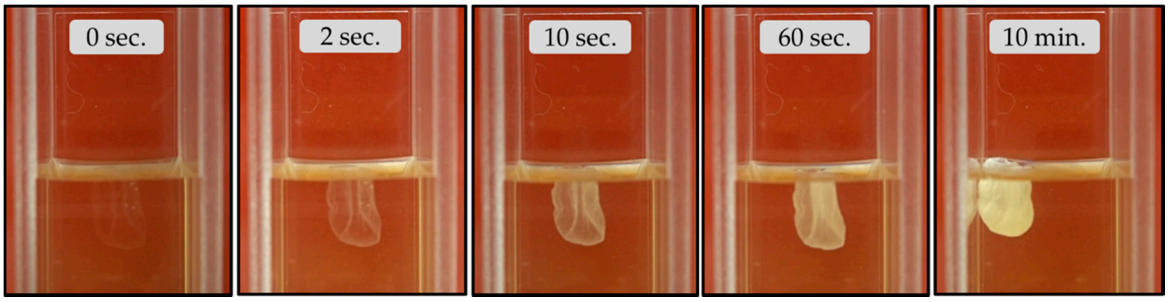

Figure 6. Temporal evolution of the morphology and texture of the barium carbonate Magadi vesicles. The width of the cuvette is 1.25 cm.

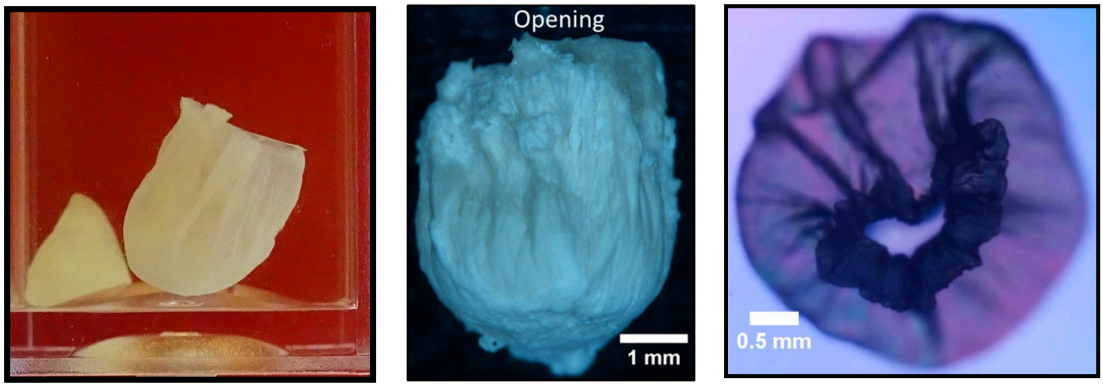

(**a**) (**b**) (**c**)

Figure 7. (**a**) Barium vesicle sinking at the bottom of the cuvette (the width of the cuvette is 1.25 cm); (**b**) corrugated surfaces of isolated barium vesicle; (**c**) hollow barium vesicle with opening.

After washing with distilled water and alcohol, the vesicles are dried and powdered for X-ray diffraction. Witherite and halite appeared in the powder X-ray diffractions (Figure 8e). Raman spectra (Figure 8f) acquired on vesicle fragments after cleaning with a similar protocol confirmed witherite [29,30]. Bands at 137, 152, and 225 cm^{-1} are assigned to lattice (external) modes whereas bands at 691 and 1061 cm^{-1} are symmetric bending and symmetric stretching modes of the carbonate groups respectively [30].

Figure 8a–d shows scanning electron micrographs of the cross-section of barium vesicles. These vesicles are ca. 18 µm thick mineral membranes (Figure 8b) composed of nano-spherical witherite aggregates. EDX analyses (Figure 8c and Figure S7) and mapping (Figure 8d and Figure S8) confirmed that the membranes are witherite, whereas the whiskers covering the inner and the outer surface of the membrane are sodium carbonate minerals (Figure 8d). A thin layer of halite precipitate on the inner and outer wall of these membranes (Figure 8d). The sodium carbonate whiskers grow outward from these halite cover. These whiskers, which appear only in SEM micrographs, could be an artefact formed by capillary evaporation during sample preparation. Figures S7 and S8 in Supplementary Materials show the EDX analyses of Figure 8c and the separate elemental maps of Figure 8d respectively.

3.2.3. Manganese Chloride Vesicles

Manganese vesicles were synthesized by adding drops of saturated manganese chloride solution on top of Magadi water. The evolution of manganese vesicles over time is presented in Figure 9a and Video S11. Figure 9a is a sequence of frames taken from Video S11 (in Supplementary Materials). The Mn salt drops suspend on the top section of the water column by retaining a bulb-like shape. In the beginning, the drops are transparent (Figure 9 at 0 sec.). After a few seconds, the color of the drops changes to white due to mineral precipitation at the interface between the drop and Magadi water,

which gives hollow vesicles. These vesicles have an opening at the very top as shown in Figure 9b. Manganese vesicles undergo visible swelling in the first 10 min and later the shape remains the same throughout the growth processes. During the active growth period (about 30 min), the vesicles suspending on the water surface rotate periodically clockwise and anti-clockwise. The opening of manganese vesicles shows corrugated surfaces that intensify from the bottom towards the mouth (Figure 9b). The development of shrinkage surfaces was accompanied by a gradual narrowing of the initially wider opening.

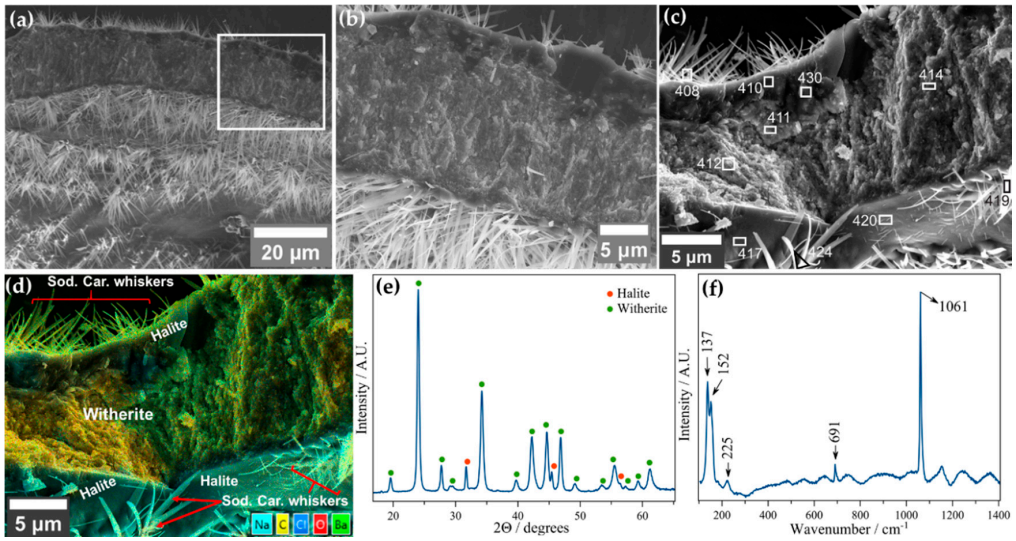

Figure 8. (**a**) Cross-section and the inner surface of Ba vesicle; (**b**) closer look of the cross-section marked by the white square in panel (**a**); (**c**) SEM micrograph of the membrane cross-section with rectangles where EDX analyses performed (see Figure S7 for EDX analyses); (**d**) EDX map of panel (**c**) showing witherite membrane with the inner and outer halite and sodium carbonate whiskers; (**e**) powder X-ray diffractogram of Ba vesicles; (**f**) Raman spectra of Ba vesicles (137, 152, 225 cm^{-1} —lattice modes; 691 cm^{-1} —symmetric bending mode; 1061 cm^{-1} —symmetric stretching mode).

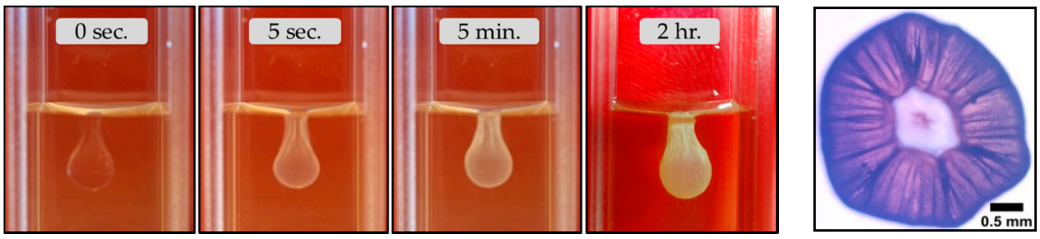

(**a**) (**b**)

Figure 9. Mineral vesicles synthesized by adding manganese chloride on Magadi water. (**a**) Growth process of the vesicles (width of the cuvette is 1.25 cm); (**b**) hollow vesicle with its opening and corrugated surfaces.

After washing with distilled water and alcohol, the vesicles are dried and powdered for X-ray diffraction. The X-ray diffraction shows halite, rhodochrosite, and nahcolite phases (Figure 10a). Raman spectra (Figure 10b) acquired on the vesicles after cleaning with a similar protocol confirmed rhodochrosite. Bands at 182 and 286 cm^{-1} are assigned to translational lattice modes whereas bands at 725 and 1087 cm^{-1} are in-plane bending and symmetric stretching modes of the carbonate groups respectively [30]. Nahcolite did not appear in Raman spectra.

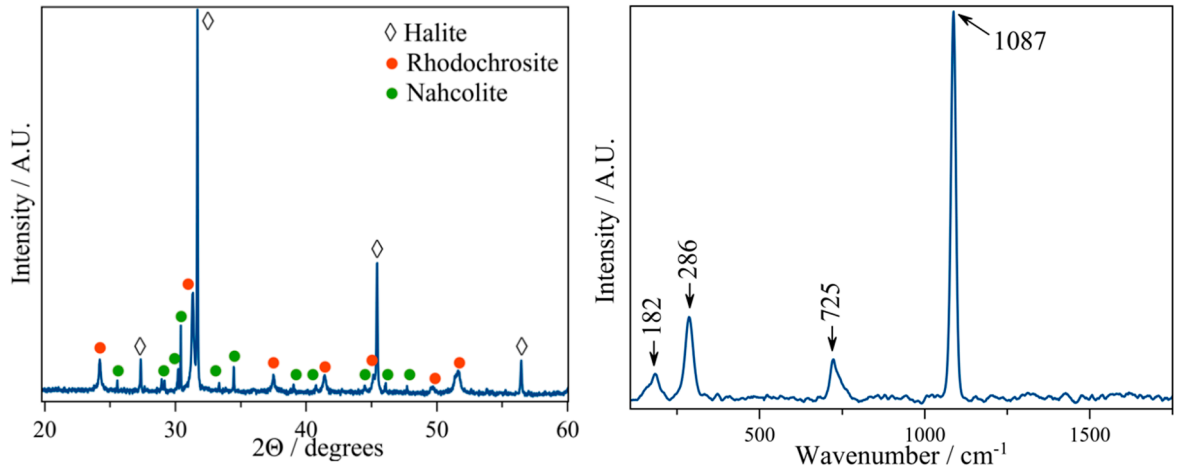

Figure 10. (**a**) Powder X-ray diffractogram; (**b**) Raman spectra of manganese vesicles (182, 286 cm^{-1} —translational lattice modes; 725 cm^{-1} —in-plane bending mode; 1087 cm^{-1} —symmetric stretching mode).

Figure 11 shows the scanning electron micrographs of manganese vesicles. As shown in Figure 11a, manganese vesicles are composed of aggregates of 9–12 µm rhodochrosite spherules. Figure 11b, with its simplified sketch (Figure 11c) shows the cross-section and the exterior of Mn membranes. EDX analysis (Figure S9) has shown that sometimes the cross-section of the manganese vesicles are covered with a smooth undulating layer of halite (Figure 11d). On top of this halite layer, spherical rhodochrosite particles precipitate (Figure 11d). The diameter of these spherules of rhodochrosite varies roughly between 1 and 3.4 µm.

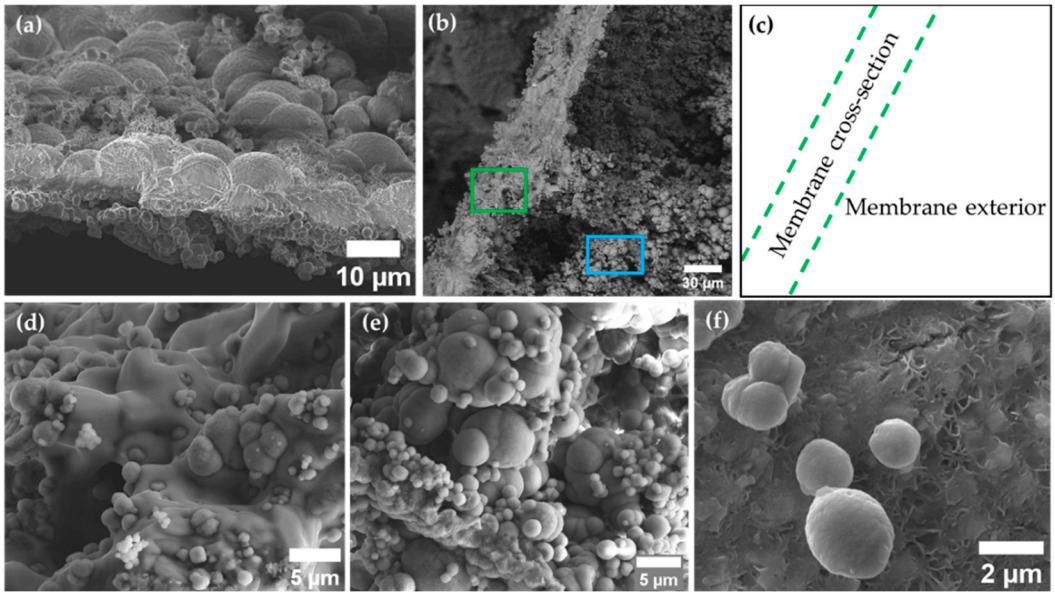

Figure 11. SEM images of manganese vesicles. (**a**) Cross-section of the membrane; (**b**) cross-section of the membrane and its exterior; (**c**) simplified sketch of panel (**b**); (**d**) closer look of the cross-section at the green rectangle in panel (**b**); (**e**) exterior of the membrane at the blue rectangle in panel (**b**); (**f**) interior wall of the membrane.

Rhodochrosite spherules with varying diameter (ca. 1–6 µm) form on the exterior of manganese membranes (Figure 11e). The interior of the membranes are covered by smooth rhodochrosite and

nahcolite on which rhodochrosite spherules precipitate (Figure 11f). Point EDX analysis of the interior surface (Figure S10) has shown negligible Cl content. Hence, the relatively higher Na on the interior surface of the membrane could be because of nahcolite that appeared in the X-ray diffractions. The spherical rhodochrosite observed at the interior and exterior section of the membrane has a smoother surface than the spherules that make the membrane.

3.2.4. Cobalt, Magnesium, Zinc, and Iron (II) Mineral Vesicles

Figure 12 and Video S12 show the growth process and morphological evolution of cobalt chloride vesicles. In the beginning, the drop with a smooth surface hangs on the uppermost layer of Magadi water. The exterior of the drop corrugates gradually following the precipitation of minerals at the interface between the Co salt drop and Magadi water, which forms the hollow mineral vesicles. Cobalt vesicles gain the final color and morphology within an hour and fall to the bottom of the cuvette. As shown in the last panel of Figure 12, cobalt vesicles have an opening on top. Hollow mineral vesicles form by using saturated cobalt nitrate solution as well. The powder X-ray diffraction of cobalt nitrate vesicles reveals $Co_2(OH)_3Cl$ and nahcolite (Figure S11).

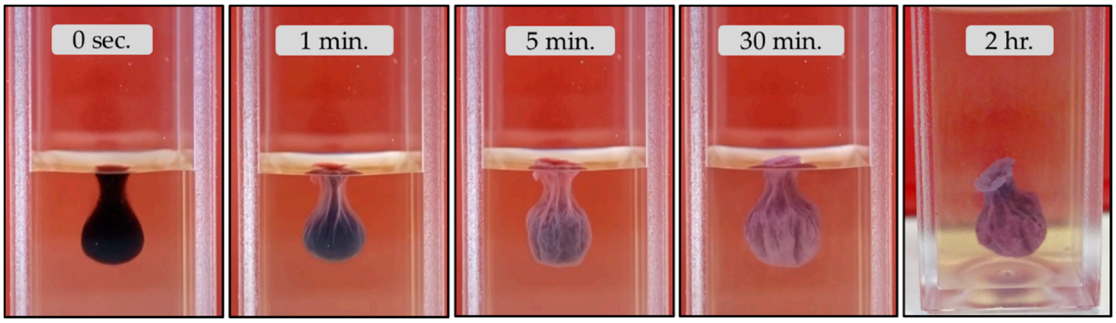

Figure 12. The growth process of cobalt chloride mineral vesicles in Magadi water.

Figure 13a and Video S13 show the growth of magnesium chloride vesicles. Figure 13a is a set of frames from Video S13. The transparent drop changes to white gradually due to mineral precipitation at the interface between the drop and Magadi water. Magnesium vesicles did not undergo visible swelling during the growth process. Osmotic pressure developed inside these vesicles, which was accommodated by the growth of a transparent dome-shaped membrane capping the opening on top as shown in Figure 13a (green arrow). This capping membrane forms when the salt solution trying to overflow out of the vesicle encounters the alkaline solution surrounding the vesicle. The overflow of the inner salt solution could be due to the vesicle's lack of expansion to accommodate the water diffusing into it. Once the membrane cap forms, the later overflow of salt solution ejects into the alkaline water due to its inability to rupture the capping membrane and forms a new vesicle (Figure 13a, blue arrow). The opening of these vesicles, therefore, serves as an osmotic pressure-relieving mechanism and inhibits membrane rupture that would form tubular membranes. Similar hollow vesicles form by using saturated magnesium sulphate drops (Figure 13b). Thenardite, blodite, loweite, and halite appear in the powder X-ray diffraction of magnesium sulphate vesicles (Figure S12).

Zinc sulphate vesicles are initially transparent like those mineral vesicles presented above and are morphologically similar to the manganese vesicles (Figure 14a). Gradually the color changes to white. During the growth process, these vesicles have a wide rupture opening that narrows down with time. The narrowing of the opening is accompanied by corrugation of the membrane (Figure 14b). Gunningite, gordaite and changoite appear in the powder X-ray diffraction of zinc sulphate vesicles (Figure S13).

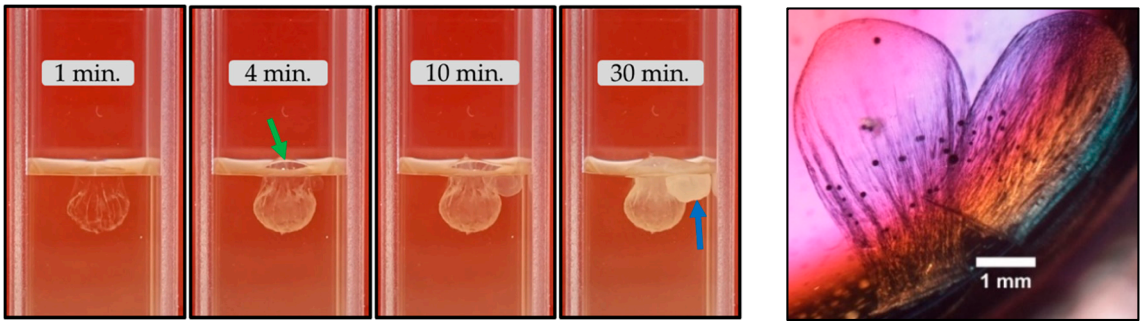

(**a**) (**b**)

Figure 13. (**a**) The growth process of magnesium chloride mineral vesicles in Magadi water (note: two vesicles grow from one drop; the width of the cuvette is 1.25 cm); (**b**) lateral view of magnesium sulphate vesicle.

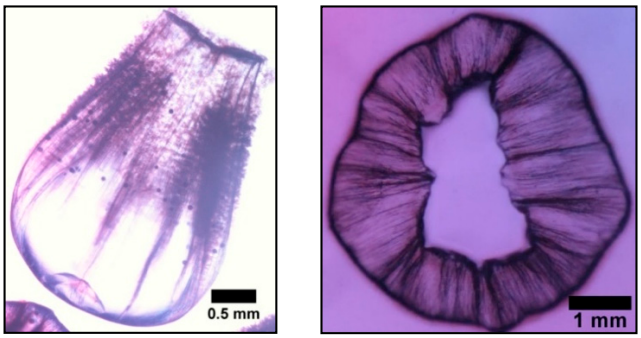

(**a**) (**b**)

Figure 14. Zinc sulphate mineral vesicle: (**a**) lateral view; (**b**) hollow vesicle with its opening.

Unlike Magadi gardens, iron (II) chloride and sulphate form hollow mineral vesicles (Figure 15 and Video S14) due to the free availability of Fe (II) in saturated solutions. These vesicles hang on the upper part of the water. The big vesicle in Figure 15a lies at the bottom because of a very shallow water column. The change in the shape of the vesicles was insignificant. The color changed from yellow to dark green. The dome-like membrane capping the opening of these vesicles is evidence of the overflow of the interior salt solution via the opening to accommodate the diffusion of water into the hollow membrane (Figure 15a, last panel). The overflowing interior solution forms very small vesicles at the bottom of the capping membrane, as in the case of the Mg vesicles (Figure 15a). Fe (II) vesicles are hollow mineral membranes (Figure 15b).

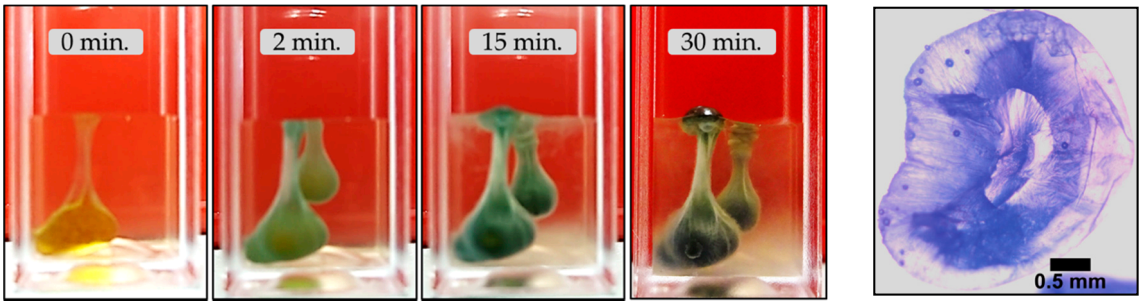

(**a**) (**b**)

Figure 15. (**a**) Growth process of iron (II) chloride vesicles. The small drop was added 25 s later (width of the cuvette is 1.25 cm); (**b**) iron (II) sulphate vesicle with its opening.

4. Discussion

The above results demonstrate that the mixing of high-pH, high-carbonate water from the soda Lake Magadi with metal salts results in the formation of membranous self-assembled structures. For the sake of clarity, we will discuss separately the two main type of experiments performed, namely a) the reactions of metal salt pellets with Magadi water, and b) the interaction of drops of a saturated solution of metal salts with Magadi water.

4.1. The Growth Process of Magadi Mineral Gardens

We have identified three groups of metals with different behavior when immersing pellets of their salt in Lake Magadi water:

1) The pellets of the less soluble and less acidic salts of Ba^{2+}, Mn^{2+} and Fe^{2+} (Table 2) do not react with the Magadi water.
2) In the case of Fe^{3+} ($FeCl_3$ and $Fe_2(SO_4)_3{\cdot}9H_2O$), Cu^{2+} ($CuCl_2{\cdot}6H_2O$ and $CuSO_4{\cdot}5H_2O$) and Zn^{2+} ($ZnCl_2$ and $ZnSO_4{\cdot}7H_2O$), the experiment resulted in the bursting of the initial membrane. The bursting of the membrane was accompanied by the bubbling of gases, and subsequent breaking of the forming mineral membranes in multiple pieces that later sediment (Videos S1–S3).
3) Unlike the aforementioned metals, the salts of Ca^{2+} ($CaCl_2{\cdot}2H_2O$) and Co^{2+} ($CoCl_2{\cdot}6H_2O$) and $Co(NO_3)_2{\cdot}6H_2O$) form tubular membranes, as shown in Figures 1 and 2 respectively. Likewise, Mg^{2+} ($MgCl_2{\cdot}6H_2O$) pellets immersed in Magadi water form mineral gardens (not presented here) that are morphologically similar to Co ($Co(NO_3)_2{\cdot}6H_2O$) gardens.

To interpret the three different behaviors of the metal salts, we should take into account two main variables, the pH of the saturated solution of these salts and their solubility in alkaline water.

The precipitation of tubular and vesicular membranes requires a reaction between the metal ions and the anionic species in the aqueous solutions. This reaction is possible when the metal salt pellets are dissolvable by the aqueous solution containing anionic species. There were no mineral precipitations from the pellets of Ba, Mn and Fe (II). However, when drops of soluble solutions of these salts were injected into the water of Magadi, both solutions react forming a metal carbonate membrane. Therefore, we can explain the absence of precipitation by the inability of the alkaline water of Lake Magadi to dissolve the pellets of the metal salts.

In the case of Fe (III), Cu and Zn, the interaction of the pellets with Magadi water resulted in extraordinary gas bubbling (see Videos S1–S3). This is due to the solubility and the extreme acidity of the solutions of these metals salts (Table 2). The metal pellets interact with the Magadi brines, the pellets dissolve and react with the brine forming a mineral membrane enveloping highly acidic metal solutions. High osmotic pressure develops inside these envelopes following the inflow of water to equilibrate the high pH and concentration gradient between the inner Fe (III), Cu and Zn solution and outer Magadi water [6,31]. The subsequent mixing of the Magadi carbonate brine with the low pH solutions shifts the initial high pH (10.9) to pH values below 8, consequently converting most carbonate and bicarbonate to carbonic acid and CO_2. CO_2 gas escapes from this quickly supersaturated solution, breaking the incipient membranes and disrupting the formation of continuous membranous structures. A similar bursting of metal-silicate hydrate membranes was observed during the growth of silica gardens with pellets of Fe (III), Cu and Zn in alkaline carbonate-rich water of Aqua de Ney springs with characteristic high pH, silica and carbonate content [9]. Note that the concentration of carbonate in Lake Magadi brines is 10-times that of Aqua de Ney water. Hence, there could be more CO_2 production and membrane disruption in Magadi than in Aqua de Ney water.

The interaction of Ca pellets with Magadi water forms a dome-like envelope in the middle of the pellets (Figure 1). This "osmotic envelope" [32] expands vertically and radially outward by a self-renewal precipitation process [32] due to high pressure inside the membranous envelope. The pressure inside the envelope develops due to osmotic-driven diffusion of water to equilibrate the concentration and pH gradient between the solutions inside and outside the envelope [6,31].

The elasticity of the envelope and slow inflow of water inhibit the bursting of the envelope and injection of the interior solution into the Magadi water. The absence of envelope rupture could be due to low CO_2 production as well. This is because of relatively less acidity than Co salts (Table 2) that form tubes by envelope rupture and inner salt jetting. Once the radial expansion ceases, transparent tubes grow horizontally from osmotic envelopes (Figure 1). The change in growth direction is likely due to the gradual rise in the density of the inner metal salt solution, which is evidenced by the vertically downward growth following the horizontal tube growth (see Figure 1g–h). The density rise could be due to further diffusion of water and subsequent dissolution of the salt pellet. For example, the Fe^{2+} concentration in the inner solution of silica garden tubes showed a marked initial increase for 10 h, reflecting the ongoing dissolution of the metal salt pellet [31].

So far, there are no reported Ca carbonate mineral gardens in natural water. However, Cardoso et al. [33] synthesized calcium gardens in commercial sodium carbonate solutions by using calcium chloride salts. The resulting membranes have vesicle forms in high sodium carbonate concentrations (1.33, 2, and 4 M), whereas at low concentration (0.5, 0.8, and 1 M), tubular gardens form [33]. The absence of envelope rupture in Magadi calcium gardens could be due to the high solute content and the high density of the water. The density of Lake Magadi brines varies mainly between 1.2 and 1.33 g/cm^3 [16,17]. The water used for the Magadi garden experiments is more concentrated than the brines reported in [16,17] and it may have a density greater than 1.2. This density is comparable with the density of silica solutions [32] reported to slow reactivity of the calcium salts in Ca-silica garden experiments. High concentration (high viscosity) silicate solution slows down the reaction and allows only a few slow-growing tubes [32]. The composition of Magadi Ca gardens include mainly calcite, gaylussite, pirssonite and minor trona. Cardoso et al. [33] reported calcite and gaylussite in Ca carbonate-hydroxide gardens.

The dissolution of Co pellets and the reaction with Magadi water form an envelope surrounding the pellets. Water diffuses into the membranous envelope to equilibrate the concentration and pH gradient between the two solutions [6,31]. Following water diffusion and a rise in internal pressure, the envelope expands and finally ruptures. At the point of rupture, the Co solution ejects into the Magadi water with the aid of buoyancy force [4,5]. Mineral precipitation at the interface between the ejected Co solution and Magadi water forms tubular membranes (Figure 2a). The tube grows in periodic pulses that give rise to the widening of the vertical tube due to the oscillation of pressure in the osmotic envelope, analogues to the growth process in budding regimes [34,35]. Due to very quick closure of the tubular membrane, osmotic pumping of the Co solution causes slow pressure build-up inside the membrane. Consequently, the growth occurs via repeated rupturing of the membrane and subsequent precipitation [5]. The oscillatory pressure is short-lived at the beginning due to the fast ejection of the inner solution. This results in the growth of small round branches at the lower part of the tube. Later, when the pH and the chemical gradient between the inner and outer solution decrease [6,31], the buoyancy of the inner solution declines and the vertical growth ends. Following the end of vertical growth, repeated rupture at the same location produces small tubes connected with the upper part of the main tubular structure [5]. The viscosity of the water could be another reason for the periodic pulses that may arise from the development of osmotic pressure that ejects the solution periodically when it reaches a critical point for penetrating the water. The buoyancy-driven ejection of Co solution forms longer tubes than Ca gardens, in which diffusion was the main driver for the expansion of the tubular mushroom-like membranes.

4.2. The Growth Process of Magadi Mineral Vesicles

Mineral precipitation triggered by pouring drops of saturated metal salt solutions in Magadi water forms hollow vesicular membranes. The formation of these mineral vesicles follows a general process that is schematically shown in Figure 16. Once the lighter metal salt drop is poured on top of the Magadi brine, the drop remains hanging on the uppermost layer of the water by a combination of buoyancy and surface tension. The shape of the liquid drop, which is controlled by its density,

is maintained for the first few seconds to few minutes (Figure 16a), depending on the onset of mineral precipitation in the interface of the metal salt drops with the surrounding Magadi water. A good example of density control over the shape of the drops is observed in Ca vesicles (Figure 3a). Initially, the liquid drop has a transparent bulb-like shape (Figure 3a at 0 min.). Water diffusion (Figure 16b) by osmosis slowly dilutes the concentration of the drop and lowers its density relative to the initial drop at 0 min. Consequently, the bottom of the drop moves upward by buoyancy effect while expanding horizontally outward, and forms a spherical transparent drop (Figure 3a at 10 min. and Figure 16c). Later on, metal carbonate minerals precipitate at the interface, forming hollow vesicles (Figure 16d), which have an opening or mouth at their uppermost edge, i.e., at the place where the metal solution is in contact with the air. This opening eventually facilitates the escape to the atmosphere of the forming CO_2 gas, thus avoiding the bursting of the membrane. The evolution over time of the shape and characteristic of the membranes depends very much of the precipitation rate, which is a function of the supersaturation of the mineral phases, and the rate of equilibration of the inner and outer regions of the vesicle, which is a function of the evolving chemical gradient between the salt solution inside the vesicle and the exterior Magadi water. The porosity and the rigidity of the forming mineral membrane allow different osmosis-driven inflows of water molecules from the alkaline water towards the metal solution inside the membrane (Figure 16d). For instance, the osmotic inflow of water and the resulting internal pressure causes the swelling of the vesicles. During swelling, the shape of the vesicles change from bulb-like to spherical membranes (Figure 16b–d). In quickly precipitating vesicles and rigid membranes, only the size of the membrane increases while retaining the initial bulb-like morphology. In Mg and Fe (II) vesicles, the rigidity of the membrane causes overflow of the interior salt solution via the mouth and precipitation of secondary vesicles upon the interaction of the overflowing interior metal solution with the exterior Magadi water (Figures 13a and 15a). Finally, the combination of the buoyancy of the drop and osmotic diffusion of water forms floating, hollow bulb-like or spherical membranes with an opening at the upper edge.

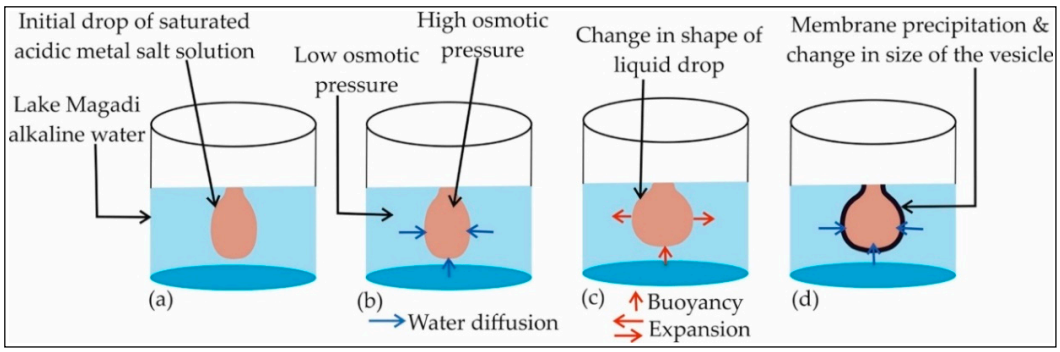

Figure 16. Illustration of the growth process of the Magadi vesicles from metal salt solution drops in Lake Magadi water.

Barium chloride drops float in Magadi water and the membranes precipitate in a few seconds. Unlike in Magadi mineral gardens, Ba vesicles form due to freely available Ba in solution. The vesicles have long-lasting corrugated surfaces and there is little change in the shape of the vesicles (Figure 6), inferring the rigidity of the membrane, unlike calcium vesicles. Among the Magadi vesicles, Ba vesicles were most stable during the preparation of SEM samples. Ba vesicles sink to the bottom in less than an hour following the intrusion of the water via the opening and subsequent rise in density of the inner solution. The density of the mineral (witherite) composing the membranes of Ba vesicles is higher than calcite and rhodochrosite. Hence, the mineral composition may play its role in sinking Ba vesicles. The composition of Ba vesicles was mainly witherite as confirmed from Raman spectra bands [29,36], EDX analysis and X-ray powder diffraction. Barium silica gardens [32] share a similar composition to the Magadi Ba vesicles. The silica garden tubes are composed of $BaCO_3$ and halite forming on the interior wall, evidencing Na+ diffusion across the membrane [32]. In the case of Ba

vesicles, the interior halite could be from a combination of Na diffusion and the intruded Na-Cl rich water via the openings, which can form halite that remained uncleaned. Trona forms in Lake Magadi due to lake surface evaporation [16]. Therefore, the minor trona in the X-ray diffraction may form during the drying of the membrane.

After pouring Mn drops onto Magadi water, manganese carbonate precipitates in a few seconds at the interface between the two solutions and forms hanging hollow membranes. Unlike in Magadi gardens, Mn vesicles form due to the availability of free Mn in solution. The swelling and rotation in the clockwise and anti-clockwise direction of Mn vesicles is evidence of the osmotic diffusion of water across the membrane. Fast membrane precipitation changes the transparent drop into a white mineral vesicle. Rapid aggregation of rhodochrosite spheres forms highly fragile vesicles. The thin layer of water near the opening may intensify the shrinkage surface of the vesicles by forming thin membranes towards the opening. The Mn-silica vesicles form by the osmotic expansion of the drop and subsequent jetting of inner salt solution due to buoyancy [23]. The composition of the Mn silica gardens and vesicles [23,37] are mainly manganese oxides and hydroxides due to the absence of CO_3, whereas Magadi Mn vesicles are mainly of rhodochrosite.

In addition to rhodochrosite, nahcolite and halite form in Magadi vesicles. Halite appeared as a smooth layer covering the membrane. The fragile nature of Mn vesicles did not allow intense cleaning and halite could precipitate during the drying of the poorly cleaned membranes. Nahcolite is a mineral predicted to form at elevated pCO_2 [38,39]. In fact, nahcolite precipitate in Little Magadi lake where the direct release of magmatic CO_2 occurs [40,41]. The interaction of acidic Mn solution (Table 2) with carbonate-rich Magadi water may release CO_2 high enough to favor nahcolite formation. CO_2 production has been already reported from the early bursting of membranes in Fe (III), Cu, and Zn silica garden experiments with carbonate-rich Aqua de Ney water [9], which is a phenomenon observed in Fe (III), Cu, and $ZnCl_2$-based Magadi vesicles.

4.3. Calcium Magadi Mineral Self-Organization and the Origin of Life

Upon the addition of Ca salt drops in Magadi water, mainly $CaCO_3$ mineral membranes precipitate at the interface between the two solutions. The evolution of the color of Ca vesicles (Figure 3a) could be due to precipitation of calcium carbonate minerals followed by halite and trona precipitation on the exterior of the membrane as observed in the EDX map of the membranes (Figure 5a). The minimal shrinkage surfaces of Ca vesicles may infer elasticity of the membrane as observed in Ca gardens. These membranous structures are selective barriers between the two distinct solutions forming a chemical gradient across the membranes. A distinct chemical gradient across the membranes [6,31] and subsequent osmotic-driven inflow of water and buoyancy-driven jetting of the acidic metal salt solutions were one of the driving mechanisms for the growth of tubular silica gardens [4,5] and carbonate-hydroxide gardens [33]. Due to the lower density of calcium salt inside the vesicle, the membranes float on the uppermost layer of the water. The chemical and pH gradient across mineral membranes causes osmotic diffusion of water into the Magadi vesicles, as evidenced from the horizontal swelling and morphological evolution from bulb-like to spherical vesicles of calcium (Figure 3a and Video S9). The morphological evolution of the drop at the beginning, while it was transparent, could be due to buoyancy that pushes the bottom of the drop to the surface following dilution of the interior solution and subsequent lowering in density. The opening on the top of the vesicles serves as a pressure-relieving mechanism, which was observed in magnesium and iron (II) chloride vesicles (Figures 13a and 15a).

Calcite, vaterite, and gaylussite minerals observed in Magadi vesicles were reported in calcium carbonate-hydroxide vesicles and gardens synthesized in sodium carbonate solution by using calcium chloride salts [33]. The halite that appeared both in the SEM images and in XRD data could be due to evaporation of Magadi water that remains uncleaned. Trona and halite commonly form during Lake Magadi surface evaporation. The spherical vateritic and calcitic morphology may arise from the transformation of spherical amorphous calcium carbonate via the routes reported in [42,43]. However,

it is important to perform time-resolved in-situ X-ray diffraction and Raman spectroscopy of the vesicles to clearly understand the mineralogical evolution during the growth process. Gaylussite is a common authigenic mineral in modern muds of Lake Magadi where local sources of calcium are available [24,44].

A recent study [15] has reported a direct correlation between phosphate and carbonate concentration values in lakes and seas. The reason is most likely due to kinetics-controlled precipitation. The supersaturation value of a given phase in solution can be defined by the equation:

$$\text{Ionic Activity Product/Solubility Product} \quad (1)$$

The solubility product of calcium phosphate is lower than that of calcium carbonate(s). Therefore, in circumneutral solutions, thermodynamically calcium phosphate precipitates first and the remaining solution is devoid of phosphate. However, at the very high carbonate concentration values of soda lakes, the saturation index of calcium carbonate can be much higher than that of calcium phosphate, thus forming gaylussite and/or calcite, sequestering excess calcium and leaving the phosphate as soluble species in the soda lake brines [15]. Similarly, our Magadi calcium mineral vesicles are composed of calcite, vaterite and gaylussite. We have confirmed by X-ray diffraction, EDX and FESEM analysis the total absence of phosphorous and calcium phosphate minerals in the Magadi vesicles and gardens, thus confirming the interesting observation that in soda lakes, carbonate minerals sequestrate Ca and prevent phosphate removal by apatite precipitation [15]. Further work is underway to a deeper exploration of this idea through analysis of phosphate in the residual water that remained after the synthesis of calcium mineral vesicles and gardens.

It has been suggested that soda lakes and alkaline silica-rich environments are analogous to early Earth's oceans [3,11–14]. Lake Magadi is analogous to hydrothermal chert environments on the Archean Earth [45,46]. The geochemical plausibility of mineral self-organization in soda lakes such as Lake Magadi infers that mineral self-assembly may have taken place on the soda oceans of early Earth. It has been reported recently that phosphate, an ion central to the origin of life and metabolism [47,48], accumulates in carbonate-rich soda lakes due to preferential calcium precipitation preventing apatite formation [15]. These phosphate-rich lakes may have preferentially formed on the prebiotic Earth [15]. It is believed that silica gardens, which catalyze the synthesis of prebiotically relevant compounds [7,23], were forming in the alkaline silica and carbonate-rich oceans of Hadean Earth [3]. The high silica, carbonate and phosphate content [3,7,15] and the plausibility of mineral self-assembly in modern soda lakes may imply that alkaline soda oceans of the early Earth could probably be the "one-pot" environments containing the important ingredients for the synthesis of prebiotically relevant molecules and plausible settings for the origin of life.

It should be noted that the contribution of silica to the precipitation of our synthesized Magadi vesicles and gardens is negligible, the membranous mineral structure being mostly made of metal carbonate precipitation. The silica content of the water collected during our field trip was not high enough for the formation of silica gardens and vesicles. The low silica content is due to two reasons. First, the samples were collected in May 2018 after an unanticipated early raining season, but more importantly, because in the last four years, all the soda lakes of the Rift Valley have experienced a raising of the water level by a few meters, the reason for which is unknown. We are performing fluid-rock interaction experiments with Magadi brines and cherts to enrich the concentration of silica to values previously reported in the literature. In addition, we are organizing a new field trip for sampling Lake Magadi during the driest season. Testing the role of silica in inducing mineral self-assembly will increase the potential of modern soda lakes to be considered as "one-pot" geochemical environments for the origin of life.

Supplementary Materials: The following are available online at http://www.mdpi.com/2073-4352/10/6/467/s1, Figure S1: Powder X-ray diffraction of mineral gardens synthesized by immersing $CaCl_2{\cdot}2H_2O$ pellets in Lake Magadi water, Figure S2: Powder X-ray diffraction of mineral gardens produced by immersing $CoCl_2{\cdot}6H_2O$ pellet in Magadi water, Figure S3: Raman spectra of mineral vesicles synthesized by adding drops of saturated $CaCl_2{\cdot}2H_2O$ solution onto Lake Magadi water, Figure S4: EDX mapping of membrane cross-section of vesicles

synthesized by adding saturated $CaCl_2{\cdot}2H_2O$ solution onto Lake Magadi water, Figure S5: EDX analysis of membrane cross-section of vesicles synthesized by adding saturated $CaCl_2{\cdot}2H_2O$ solution onto Lake Magadi water, Figure S6: EDX analysis of calcium mineral membrane cross-section containing gaylussite, Figure S7: EDX analysis of membrane cross-section of vesicles synthesized by adding saturated $BaCl_2{\cdot}2H_2O$ solution onto Lake Magadi water, Figure S8: EDX mapping of membrane cross-section of vesicles synthesized by adding saturated $BaCl_2{\cdot}2H_2O$ solution onto Lake Magadi water, Figure S9: EDX analysis of the cross-section of mineral vesicles synthesized by adding saturated $MnCl_2{\cdot}4H_2O$ solution onto Magadi water, Figure S10: EDX analysis of the interior surface of mineral vesicles synthesized by adding saturated $MnCl_2{\cdot}4H_2O$ solution onto Magadi water, Figure S11: Powder X-ray diffraction of mineral vesicles synthesized by adding saturated $Co(NO_3)_2{\cdot}6H_2O$ solution onto Lake Magadi water, Figure S12: Powder X-ray diffraction of mineral vesicles synthesized by adding saturated $MgSO_4$ solution onto Lake Magadi water, Figure S13: Powder X-ray diffraction of mineral vesicles synthesized by adding saturated $ZnSO_4{\cdot}7H_2O$ solution onto Lake Magadi water, Video S1: Gas bubbling and bursting of reaction products of the $FeCl_3$ pellet and Magadi water, Video S2: Gas bubbling and bursting of reaction products of the $CuCl_2{\cdot}6H_2O$ pellet and Magadi water, Video S3: Gas bubbling and bursting of reaction products of the $ZnCl_2$ pellet and Magadi water, Video S4: Growth process of mineral gardens by the interaction of the $CaCl_2{\cdot}2H_2O$ pellet with Magadi water, Video S5: Growth process of mineral gardens by the interaction of the $Co(NO_3)_2{\cdot}6H_2O$ salt pellet with Magadi water, Video S6: Gas bubbling and bursting upon the reaction of drops of saturated $FeCl_3$ solution and Magadi water, Video S7: Gas bubbling and bursting upon the reaction of drops of saturated $CuCl_2{\cdot}6H_2O$ solution and Magadi water, Video S8: Gas bubbling and bursting upon the reaction of drops of saturated $ZnCl_2$ solution and Magadi water, Video S9: Synthesis of mineral vesicles by adding saturated $CaCl_2{\cdot}2H_2O$ solution onto Magadi water, Video S10: Synthesis of mineral vesicles by adding saturated $BaCl_2{\cdot}2H_2O$ solution onto Magadi water, Video S11: Synthesis of mineral vesicles by adding saturated $MnCl_2{\cdot}4H_2O$ solution onto Magadi water, Video S12: Synthesis of mineral vesicles by adding saturated CoCl2·6H2O solution onto Magadi water, Video S13: Synthesis of mineral vesicles by adding saturated $MgCl_2{\cdot}6H_2O$ solution onto Magadi water, Video S14: Synthesis of mineral vesicles by adding saturated $FeCl_2{\cdot}4H_2O$ solution onto Magadi water.

Author Contributions: M.G. performed the experiments, characterized the materials and analyzed the results; J.M.G.-R. conceived and designed the experiments and analyzed the results; C.V.-E. performed X-ray diffraction experiments and mineral phase identification; I.G.-T. performed the SEM study and EDX analyses; M.G. and J.M.G.-R. wrote the paper. All authors have read and agreed to the published version of the manuscript.

Funding: The authors thank the European Research Council under the European Union's seventh Framework Program (FP7/2007-2013)/ERC grant agreement no. 340863 and the Spanish "Ministerio de Educacion y Ciencia" for the financial support to the project CGL2016-78971-P. MG. acknowledges Grant No. BES-2017-081105 of the "Ministerio de Ciencia, Innovacion y Universidades" of the Spanish government.

Acknowledgments: The authors thank Alicia González Segura for help with the scanning electron microscope, Francisca Espinosa, Raquel Fernandez-Penas, and Joaquín Criado-Reyes for technical help in the laboratory. We also thank National Commission for Science Technology and Information, National Environmental Management Authority and Kenya Wildlife Services for research permissions. Magadi Tata Chemicals Ltd. and National Museums of Kenya provide logistic help. Finally, we also acknowledge very much Patricia Gitari, Lukas Sossoika, and Tara Barwa for their assistance in fieldwork.

Conflicts of Interest: The authors declare no conflict of interest.

References

1. García-Ruiz, J.M.; Otálora, F. Crystal Growth in Geology: Patterns on the Rocks. In *Handbook of Crystal Growth*; Nishinaga, T., Rudolph, P., Eds.; Elsevier: Amsterdam, The Netherlands, 2015; Volume II, pp. 1–43. [CrossRef]
2. Nakouzi, E.; Steinbock, O. Self-organization in precipitation reactions far from the equilibrium. *Sci. Adv.* **2016**, *2*, e1601144. [CrossRef] [PubMed]
3. García-Ruiz, J.M.; van Zuilen, M.; Bach, W. Mineral self-organization on a lifeless planet. *Phys. Life Rev.* **2020**. (in press). [CrossRef]
4. Kellermeier, M.; Glaab, F.; Melero-García, E.; García-Ruiz, J.M. Experimental Techniques for the Growth and Characterization of Silica Biomorphs and Silica Gardens. In *Methods in Enzymology*; De Yoreo, J.J., Ed.; Academic Press: Cambridge, MA, USA, 2013; Volume 532, pp. 225–256. [CrossRef]
5. Barge, L.M.; Cardoso, S.S.S.; Cartwright, J.H.E.; Cooper, G.J.T.; Cronin, L.; De Wit, A.; Doloboff, I.J.; Escribano, B.; Goldstein, R.E.; Haudin, F.; et al. From Chemical Gardens to Chemobrionics. *Chem. Rev.* **2015**, *115*, 8652–8703. [CrossRef] [PubMed]
6. Glaab, F.; Kellermeier, M.; Kunz, W.; Morallon, E.; García-Ruiz, J.M. Formation and Evolution of Chemical Gradients and Potential Differences Across Self-Assembling Inorganic Membranes. *Angew. Chemie* **2012**, *124*, 4393–4397. [CrossRef]

7. Saladino, R.; Di Mauro, E.; García-Ruiz, J.M. A Universal Geochemical Scenario for Formamide Condensation and Prebiotic Chemistry. *Chem. A Eur. J.* **2019**, *25*, 3181–3189. [CrossRef]
8. Satoh, H.; Tsukamoto, K.; Garcia-Ruiz, J.M. Formation of chemical gardens on granitic rock: A new type of alteration for alkaline systems. *Eur. J. Mineral.* **2014**, *26*, 415–426. [CrossRef]
9. García-Ruiz, J.M.; Nakouzi, E.; Kotopoulou, E.; Tamborrino, L.; Steinbock, O. Biomimetic mineral self-organization from silica-rich spring waters. *Sci. Adv.* **2017**, *3*, e1602285. [CrossRef]
10. García-Ruiz, J.M. Carbonate precipitation into alkaline silica-rich environments. *Geology* **1998**, *26*, 843–846. [CrossRef]
11. Kempe, S.; Degens, E.T. An early soda ocean? *Chem. Geol.* **1985**, *53*, 95–108. [CrossRef]
12. Kempe, S.; Kazmierczak, J.; Degens, E.T. The Soda Ocean Concept and Its Bearing on Biotic Evolution. In *Origin, Evolution, and Modern Aspects of Biomineralization in Plants and Animals*; Crick, R.E., Ed.; Springer: Boston, MA, USA, 1989; pp. 29–43.
13. García-Ruiz, J.M. Geochemical Scenarios for the Precipitation of Biomimetic Inorganic Carbonates. In *Carbonate Sedimentation and Diagenesis in the Evolving Precambrian World*; Grotzinger, J.P., James, N.P., Eds.; SEPM Society for Sedimentary Geology: Tulsa, OK, USA, 2000; Volume 67, pp. 75–89.
14. Kempe, S.; Kazmierczak, J. Soda Ocean Hypothesis. In *Encyclopedia of Geobiology*; Reitner, J., Thiel, V., Eds.; Springer: Dordrecht, The Netherlands, 2011; pp. 829–833.
15. Toner, J.D.; Catling, D.C. A carbonate-rich lake solution to the phosphate problem of the origin of life. *Proc. Natl. Acad. Sci. USA* **2020**, *117*, 883–888. [CrossRef]
16. Eugster, H.P. Chemistry and origin of the brines of Lake Magadi, Kenya. *Miner. Soc. Amer. Spec. Pap.* **1970**, *3*, 213–235.
17. Jones, B.F.; Eugster, H.P.; Rettig, S.L. Hydrochemistry of the Lake Magadi basin, Kenya. *Geochim. Cosmochim. Acta* **1977**, *41*, 53–72. [CrossRef]
18. Baker, B.H. *Geology of the Magadi Area*; Geological Survey of Kenya: Nairobi, Kenya, 1958; Volume 42, p. 81.
19. Baker, B.H. *Geology of the Area south of Magadi*; Geological Survey of Kenya: Nairobi, Kenya, 1963; Volume 61, p. 27.
20. Deocampo, D.M.; Renaut, R.W. Geochemistry of African Soda Lakes. In *Soda Lakes of East Africa*; Schagerl, M., Ed.; Springer: Cham, Switzerland, 2016; pp. 77–93.
21. Garrels, R.M.; Mackenzie, F.T. Origin of the Chemical Compositions of Some Springs and Lakes. In *Equilibrium Concepts in Natural Water Systems*; Stumm, W., Ed.; ACS: Washington, DC, USA, 1967; pp. 222–242. [CrossRef]
22. Hardie, L.A.; Eugster, H.P. The Evolution of Closed-Basin Brines. *Miner. Soc. Amer. Spec. Pap.* **1970**, *3*, 273–290.
23. Mattia Bizzarri, B.; Botta, L.; Pérez-Valverde, M.I.; Saladino, R.; Di Mauro, E.; García-Ruiz, J.M. Silica Metal Oxide Vesicles Catalyze Comprehensive Prebiotic Chemistry. *Chem. A Eur. J.* **2018**, *24*, 8126–8132. [CrossRef]
24. Eugster, H.P. Lake Magadi, Kenya, and Its Precursors. In *Developments in Sedimentology*; Nissenbaum, A., Ed.; Elsevier: Amsterdam, The Netherlands, 1980; Volume 28, pp. 195–232. [CrossRef]
25. Jones, B.F.; Rettig, S.L.; Eugster, H.P. Silica in Alkaline Brines. *Science* **1967**, *158*, 1310–1314. [CrossRef]
26. Haynes, W.M. (Ed.) *CRC Handbook of Chemistry and Physics*, 97th ed.; CRC Press: Boca Raton, FL, USA, 2016; ISBN 978-1-4987-5429-3.
27. Bischoff, W.D.; Sharma, S.K.; MacKenzie, F.T. Carbonate ion disorder in synthetic and biogenic magnesian calcites: A Raman spectral study. *Am. Mineral.* **1985**, *70*, 581–589.
28. Urmos, J.; Sharma, S.K.; Mackenzie, F.T. Characterization of some biogenic carbonates with Raman spectroscopy. *Am. Mineral.* **1991**, *76*, 641–646.
29. Burgio, L.; Clark, R.J. Library of FT-Raman spectra of pigments, minerals, pigment media and varnishes, and supplement to existing library of Raman spectra of pigments with visible excitation. *Spectrochim. Acta Part. A Mol. Biomol. Spectrosc.* **2001**, *57*, 1491–1521. [CrossRef]
30. Frezzotti, M.L.; Tecce, F.; Casagli, A. Raman spectroscopy for fluid inclusion analysis. *J. Geochemical Explor.* **2012**, *112*, 1–20. [CrossRef]
31. Glaab, F.; Rieder, J.; García-Ruiz, J.M.; Kunz, W.; Kellermeier, M. Diffusion and precipitation processes in iron-based silica gardens. *Phys. Chem. Chem. Phys.* **2016**, *18*, 24850–24858. [CrossRef]
32. Cartwright, J.H.E.; Escribano, B.; Khokhlov, S.; Sainz-Díaz, C.I. Chemical gardens from silicates and cations of group 2: A comparative study of composition, morphology and microstructure. *Phys. Chem. Chem. Phys.* **2011**, *13*, 1030–1036. [CrossRef]

33. Cardoso, S.S.S.; Cartwright, J.H.E.; Sainz-Díaz, C.I. Carbonate-hydroxide chemical-garden tubes in the soda ocean of Enceladus: Abiotic membranes and microtubular forms of calcium carbonate. *Icarus* **2019**, *319*, 337–348. [CrossRef]
34. Thouvenel-Romans, S.; Steinbock, O. Oscillatory growth of silica tubes in chemical gardens. *J. Am. Chem. Soc.* **2003**, *125*, 4338–4341. [CrossRef]
35. Thouvenel-Romans, S.; Van Saarloos, W.; Steinbock, O. Silica tubes in chemical gardens: Radius selection and its hydrodynamic origin. *Europhys. Lett.* **2004**, *67*, 42–48. [CrossRef]
36. Lafuente, B.; Downs, R.T.; Yang, H.; Stone, N. The power of databases: The RRUFF project. In *Highlights in Mineralogical Crystallography*; Armbruster, T., Danisi, R.M., Eds.; De Gruyter: Berlin, Germany, 2016; pp. 1–29.
37. Cartwright, J.H.E.; Escribano, B.; Sainz-Díaz, C.I. Chemical-Garden Formation, Morphology, and Composition. I. Effect of the Nature of the Cations. *Langmuir* **2011**, *27*, 3286–3293. [CrossRef]
38. Lowenstein, T.K.; Demicco, R.V. Elevated Eocene Atmospheric CO_2 and Its Subsequent Decline. *Science* **2006**, *313*, 1928. [CrossRef]
39. Jagniecki, E.A.; Lowenstein, T.K. Evaporites of the Green River Formation, Bridger and Piceance Creek Basins: Deposition, Diagenesis, Paleobrine Chemistry, and Eocene Atmospheric CO_2. In *Stratigraphy and Paleolimnology of the Green River Formation, Western USA*; Smith, M.E., Carroll, A.R., Eds.; Springer: Dordrecht, The Netherlands, 2015; pp. 277–312.
40. Lee, H.; Muirhead, J.D.; Fischer, T.P.; Ebinger, C.J.; Kattenhorn, S.A.; Sharp, Z.D.; Kianji, G. Massive and prolonged deep carbon emissions associated with continental rifting. *Nat. Geosci.* **2016**, *9*, 145–149. [CrossRef]
41. Lowenstein, T.K.; Jagniecki, E.A.; Carroll, A.R.; Smith, M.E.; Renaut, R.W.; Owen, R.B. The Green River salt mystery: What was the source of the hyperalkaline lake waters? *Earth-Science Rev.* **2017**, *173*, 295–306. [CrossRef]
42. Rodriguez-Blanco, J.D.; Shaw, S.; Benning, L.G. The kinetics and mechanisms of amorphous calcium carbonate (ACC) crystallization to calcite, via vaterite. *Nanoscale* **2011**, *3*, 265–271. [CrossRef]
43. Bots, P.; Benning, L.G.; Rodriguez-Blanco, J.-D.; Roncal-Herrero, T.; Shaw, S. Mechanistic Insights into the Crystallization of Amorphous Calcium Carbonate (ACC). *Cryst. Growth Des.* **2012**, *12*, 3806–3814. [CrossRef]
44. Surdam, R.C.; Eugster, H.P. Mineral reactions in the sedimentary deposits of the Lake Magadi region, Kenya. *Geol. Soc. Am. Bull.* **1976**, *87*, 1739. [CrossRef]
45. Eugster, H.P.; Jones, B.F. Gels Composed of Sodium-Aluminium Silicate, Lake Magadi, Kenya. *Science* **1968**, *161*, 160–163. [CrossRef]
46. Reinhardt, M.; Goetz, W.; Duda, J.-P.; Heim, C.; Reitner, J.; Thiel, V. Organic signatures in Pleistocene cherts from Lake Magadi (Kenya) – implications for early Earth hydrothermal deposits. *Biogeosciences* **2019**, *16*, 2443–2465. [CrossRef]
47. Pasek, M.A.; Gull, M.; Herschy, B. Phosphorylation on the early earth. *Chem. Geol.* **2017**, *475*, 149–170. [CrossRef]
48. Plattner, H.; Verkhratsky, A. Inseparable tandem: Evolution chooses ATP and Ca^{2+} to control life, death and cellular signalling. *Philos. Trans. R. Soc. B Biol. Sci.* **2016**, *371*, 20150419. [CrossRef]